SIMULATION OF SEMICONDUCTOR DEVICES AND PROCESSES Vol. 4
Edited by W. Fichtner, D. Aemmer - Zurich (Switzerland) September 12-14, 1991 - Hartung-Gorre

Operation of Vertical and Lateral Dual Collector Magnetotransistors Studied by Exact 2D-Simulation

Concetta Riccobene, Gerhard Wachutka, and Henry Baltes
Physical Electronics Laboratory, ETH-Hönggerberg, HPT
CH-8093 Zurich, Switzerland

Josef Bürgler
Integrated Systems Laboratory, ETH-Zentrum
CH-8092 Zurich, Switzerland

Abstract

Dual collector magnetotransistors are used as magnetic field sensors in many practical applications. However, up to now the details of the sensor operation have not completely been understood and, hence, an optimized sensor design is achieved by trial and error rather than by systematic design rules. To gain insight which phenomena primarily determine the magnetic field sensitivity and which parasitic effects deteriorate the device performance, we studied the galvanomagnetic carrier transport in vertical and lateral integrated transistors by means of exact two-dimensional modeling of the complete device structures in their full extension.

Our simulations demonstrate that, in the case of the vertical transistors, it is essentially the much disputed emitter injection modulation effect which is decisive for the sensor response. In the case of the lateral transistor, our results reveal that the sensitivity is determined by an involved interplay of minority- and majority-carrier deflection, injection modulation, and magnetoconcentration. By comparison of several device structures differing in the doping profile and the emitter-collector spacing the trade-off between high sensitivity and low noise level of the sensor response is discussed.

1 General Aspects

Magnetic-field-sensitive integrated bipolar transistors serve as input transducers which convert a magnetic field $\vec{B}$ into an electronic signal [1]. They are used in an increasing variety of applications [2] such as control of magnetic apparatus, recognition of magnetic patterns on tapes, disks, and credit cards, potential-free current detection, and contactless measurement of electric power. Integrated magnetotransistors provide the advantage that, on the same semiconductor chip, the sensor element may be monolithically combined with the circuitry necessary for signal conditioning and error compensation. Thus, using standard IC technologies, the inexpensive batch fabrication of highly reliable sensors of small overall size can be achieved. However, up to now many details of the sensor operation have not completely been understood and, hence, an optimized sensor design is often obtained by trial and error rather than by systematic application of established design rules.

This motivated us to study the galvanomagnetic carrier transport in integrated magnetotransistors using exact two-dimensional numerical simulation. We considered two different types of

devices, *vertical* (Fig. 1) and *lateral* (Figs. 7–8) dual collector magnetotransistors as obtained by industrial silicon technology [3,4]. Under the action of a magnetic field $\vec{B}$ applied parallel to the surface of the transistors (i.e., perpendicular to the two-dimensional cross-sections shown in Figs. 1–14 and 17-24), an imbalance between the two collector currents, I_{C_1} and I_{C_2}, is caused. Measuring the difference current $I_{C_1} - I_{C_2}$ allows to determine the magnitude of the magnetic field $|\vec{B}|$ according to

$$I_{C_1} - I_{C_2} = S\,|\vec{B}|\,(I_{C_1} + I_{C_2}) \tag{1}$$

where S denotes the sensitivity of the device.

2 Basic Model Equations

In order to gain insight which factors primarily influence the sensitivity and contribute to parasitic quantities such as the substrate current, we set up and solved the transport equations governing the flow of electrons (n) and holes (p) in the interior of a magnetic device. To this end, the widely used drift-diffusion-based model of the carrier current densities $\vec{J}_n$ and $\vec{J}_p$ has to be augmented by magnetic-field-dependent terms allowing for the deflection of the carriers due to the *Lorentz force* [5,6]:

$$\vec{J}_\alpha = -\underline{\sigma}_\alpha \nabla\phi_\alpha - \underline{\sigma}_\alpha \frac{1}{1+(\mu_\alpha^* B)^2}\left[\mu_\alpha^* \vec{B} \times \nabla\phi_\alpha + \mu_\alpha^* \vec{B} \times (\mu_\alpha^* \vec{B} \times \nabla\phi_\alpha)\right] \quad ; \quad \alpha = n, p \tag{2}$$

Here, $\underline{\sigma}_\alpha$ denotes the electric conductivity of the respective carrier type, μ_α^* the Hall mobility, and ϕ_α is the quasi-Fermi potential. The complete set of dynamic equations consists of these current relations together with the particle balance equations

$$\frac{\partial n}{\partial t} = \frac{1}{q}\, div\, \vec{J}_n + G - R \quad ; \quad \frac{\partial p}{\partial t} = -\frac{1}{q}\, div\, \vec{J}_p + G - R \tag{3}$$

(n, p : carrier concentrations; G, R : generation and recombination rates; q : elementary charge) and Poisson's equation

$$div(\epsilon \nabla\psi) = q\,(N_A^- - N_D^+ + n - p) \tag{4}$$

(ψ : electric potential; ϵ : permittivity constant; N_A^-, N_D^+ : concentrations of ionized acceptors and donors, respectively).
With a magnetic field $\vec{B}$ acting on the device, the boundary condition for the electric potential ψ along a non-contacted outer boundary portion of a semiconductor region reads

$$\left.\frac{\partial\psi}{\partial N}\right|_{sc} = -\rho_{surf} + \sigma R(\vec{B} \times \nabla\psi) \cdot \vec{N} \tag{5}$$

where $\vec{N}$ is the outward unit normal vector, ρ_{surf} is the surface charge

$$\sigma = \sigma_n + \sigma_p \tag{6}$$

is the ambipolar electric conductivity, and

$$R = \frac{\sigma_n^2 R_n + \sigma_p^2 R_p}{\sigma^2} \tag{7}$$

denotes the ambipolar Hall coefficient (R_α : Hall coefficient of carrier type α).
If the magnetic field $\vec{B}$ points in a direction perpendicular to $\vec{N}$, this equation states the well-known fact that the electric field $-\nabla\psi$ is tilted by the *Hall angle* θ according to the relation

$$tan\,\theta = \sigma R|\vec{B}|\,. \tag{8}$$

The boundary conditions along internal interfaces or contacted outer surface portions are not affected by the magnetic field.

For the numerical calculations an implementation of eqns. (2)–(5) in the general purpose 2D-device simulator *GENSIM* [7] was used. The discretization of the device equations was performed on a non-uniform triangular grid adapted to the doping profile, using the box integration method in combination with the Scharfetter-Gummel interpolation scheme [8]. The numerical incorporation of the galvanomagnetic effect follows the ideas described in [9]. In contrast to previous work [6], the complete device structures in their full extension without any restrictions and simplifications were modeled.

3 Results

3.1 Vertical Magnetotransistor

In the *vertical magnetotransistor* (Fig. 1) the n^+-emitter and the p-base region are embedded in a n-doped epi-layer serving as collector with two separate contacts C_1 and C_2. When operated in active mode ($V_{CE} = 5\,V$, $I_B = 10\,\mu A$), a considerable hole current flows from the two base contacts B_1 and B_2 along the base-emitter junction in between and diffuses into the emitter (Fig. 2). Without magnetic field, the hole current distribution is completely symmetric and, consequently, initiates a symmetric injection of electrons into the base which, after reaching the collector, carry equal portions of current to the contacts C_1 and C_2. Under the influence of the Lorentz force at non-zero magnetic field, the hole current flowing from the right or left base contact, respectively, to the emitter is slightly enhanced underneath the one half of the emitter region and diminished underneath the other half. (Fig. 3). This results in a lateral modulation of the electron current density emanating from the emitter into base and collector (Fig. 4). Thus the *emitter injection modulation* model is fully confirmed by our results. The asymmetry of current flow is augmented by the action of majority-carrier deflection in the epi-zone where, due to the low doping, the carrier transport is drift-aided by a nearly one-dimensional lateral electric field (Fig. 5). However, this effect is partly cancelled by the Hall field developing across the epi-zone (Fig. 6). Hence we conclude that the imbalance of the collector currents is primarily induced within a rather confined vicinity of the emitter-base junction. Consequently, a small portion of the device only contributes to the sensitivity which, therefore, is limited to some percent per Tesla. On the other hand, it is the localized influence of the magnetic field on the base current that leads to a favorable correlation of the noise levels of the collector currents [3,10]. Operating the magnetotransistor in differential mode, the noise correlation can be exploited to obtain an enhanced signal-to-noise ratio.

Figures: Vertical Magnetotransistor

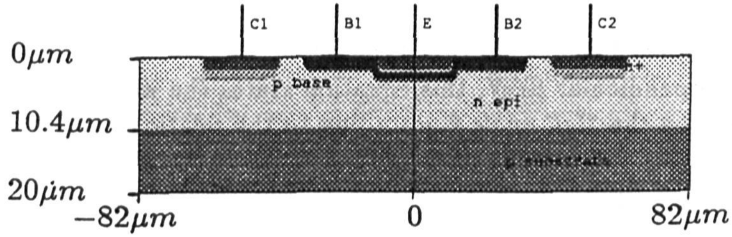

Fig. 1: Device structure (doping profile).

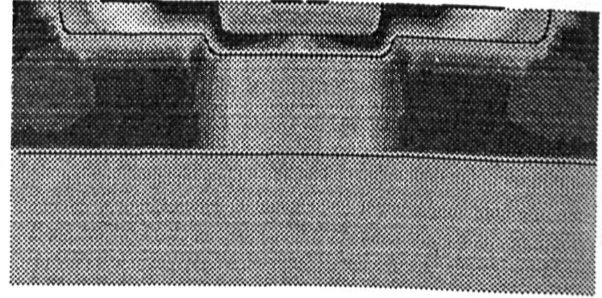

Fig. 2: Hole current density ($\vec{B} = 0$).

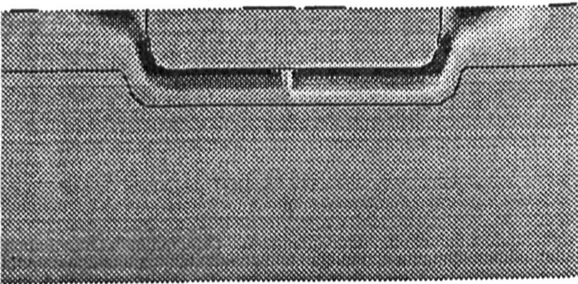

Fig. 3: Change of hole current density at $B = 0.35\,T$.

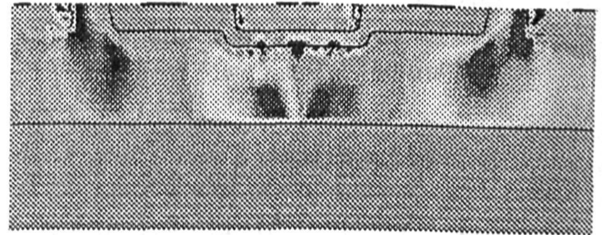

Fig. 4: Change of electron current density at $B = 0.35\,T$.

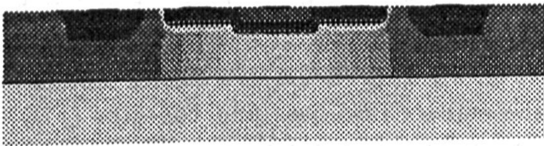

Fig. 5: Electric potential ($\vec{B} = 0$).

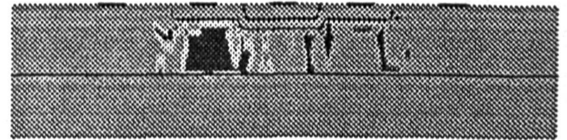

Fig. 6: Hall voltage ($B = 0.35\,T$).

3.2 Lateral Magnetotransistor

In the *lateral magnetotransistor* (Figs. 7–8) the n-epi-layer together with a n^+-doped buried layer constitute the base region. Three p^+-diffusions serve as the common emitter E and the two collectors C_1 and C_2. The emitter is surrounded by a floating n^+-guard-ring used for suppressing sidewall injection. By the circuit designer it is favored to have the p-substrate contacts S_1 and S_2 on the same potential as the collectors ($V_{CE} = -5\,V$); unfortunately this implies a high substrate current through the parasitic *pnp*-transistor formed by emitter, base, and substrate. The buried layer is intended to impair the current gain of this transistor and, thereby, to reduce the current noise level caused by the substrate current. However, by variation of the lateral width of the buried layer and the emitter-collector spacing we find that, with the technology considered, an incomplete shielding of the substrate can be achieved only (Tab. 1). Even in the case that the buried layer covers the full base-emitter distance (Fig. 7), a substantial portion of the hole current injected by the emitter is able to penetrate the buried layer (Fig. 13). Thus the substrate current cannot be reduced to less than about $8 - 16\,\%$ of the collector current, and it does not decrease more than by a factor of 10 in comparison with the buried layer confined to the area underneath the emitter (Fig. 14 and Tab. 1).

Two interesting results follow from the fact that the buried layer and the guard-ring act as shunts in the high-ohmic epi-zone (Figs. 9–10). The first consequence is reflected in the I_B *vs.* V_{BE} characteristics (Fig. 15) showing that, with the extended buried layer, there is a relatively low base-emitter resistance, because the electron flow from the base contacts to the emitter is almost completely conducted through the low-ohmic buried layer (Fig. 11). In the case of the confined buried layer, the base-emitter resistance is considerably higher, since it is composed of a high-ohmic portion underneath the base contact and the collector in series with the buried layer and the guard-ring. Accordingly, after traversing the drift-dominated high-ohmic region, the base-emitter current takes its path partly through the buried layer and partly past the layer through the guard-ring to the emitter.

As second consequence from the high electric conductivity of the buried layer, it follows that the formation of a Hall field is efficiently suppressed (Figs. 17–18). Therefore, both *minority- and majority-carrier deflection* occur in the base region and determine the sensitivity by their interplay. Figs. 19–20 show the change of the electron current density as caused by the action of the Lorentz force; a magnetic field $B = 1\,T$ induces a maximum asymmetry in the base current density of about $20\,\%$. The resulting imbalance of the electron concentration in the vicinity of the emitter-base junction (Figs. 21–22) leads to an asymmetric injection of holes analogous to the above-discussed injection modulation in the vertical transistor. One should note, however, that in the lateral transistor this effect is basically a side-effect of majority-carrier deflection of the base currents and, hence, its origin is not localized in a vicinity of the emitter.

In the transistor with the confined buried layer, we find also a magnetic field-induced modulation of the spreading resistance in the high-ohmic part of the base (*magnetoconcentration effect*). The resulting change in the voltage drop along this region is displayed in Fig. 18. One should note that magnetoconcentration is not possible in the case of the extended buried layer, since there is no drift-governed part of the base which is shared by both types of carriers.

The third mechanism, which is crucial or even predominant for the magnetic field sensitivity, consists in (partly drift-aided) minority-carrier deflection of the emitter-collector and emitter-substrate currents (Figs. 23–24). Consequently, the sensitivity is enhanced by enlarging the emitter-collector spacing and, thereby, the length of the drift-governed portion of the current paths along which the injected holes are particularly deflected by the magnetic field (cf. Fig. 16). By the same argument, the sensitivity increases if the lateral width of the buried layer is reduced,

Figures: Lateral Magnetotransistor

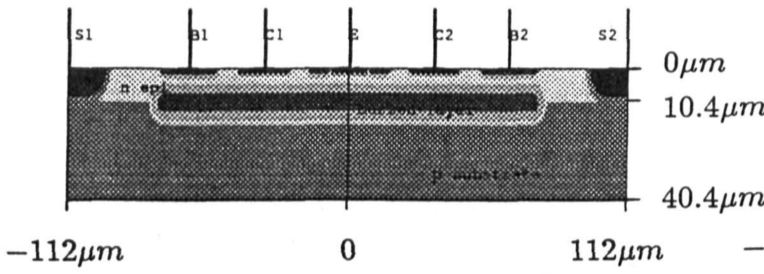

Fig. 7: Device structure (doping) with extended buried layer.

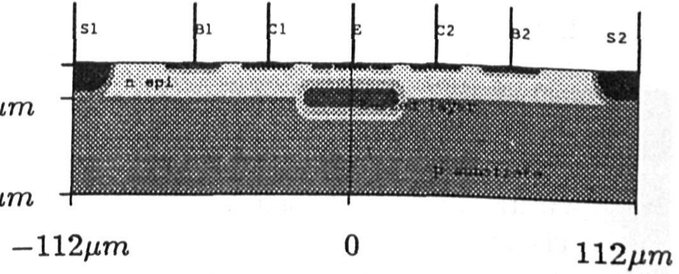

Fig. 8: Device structure (doping) with confined buried layer.

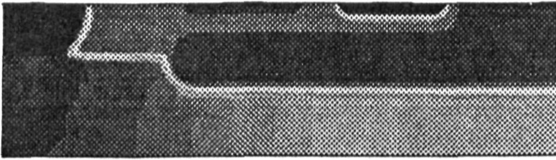

Fig. 9: Electric potential (extended b.l., $\vec{B} = 0$).

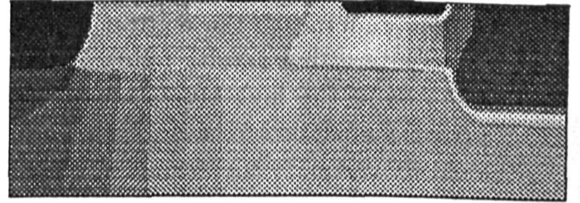

Fig. 10: Electric potential (confined b.l., $\vec{B} = 0$).

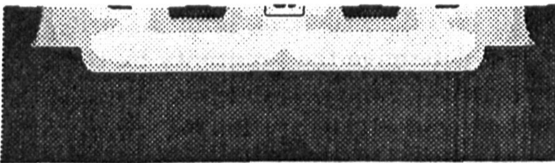

Fig. 11: Electron current density (extended b.l., $\vec{B} = 0$).

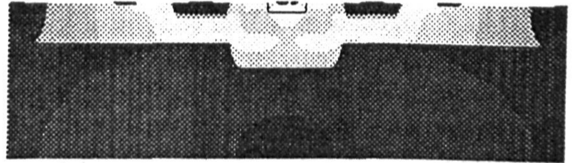

Fig. 12: Electron current density (confined b.l., $\vec{B} = 0$).

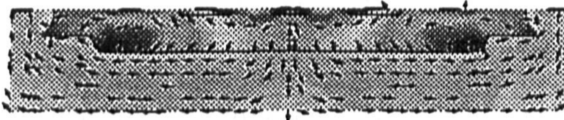

Fig. 13: Hole current density (extended b.l., $\vec{B} = 0$).

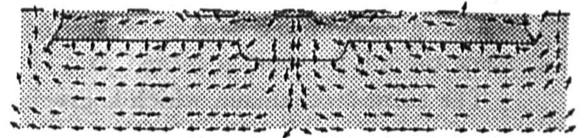

Fig. 14: Hole current density (confined b.l., $\vec{B} = 0$).

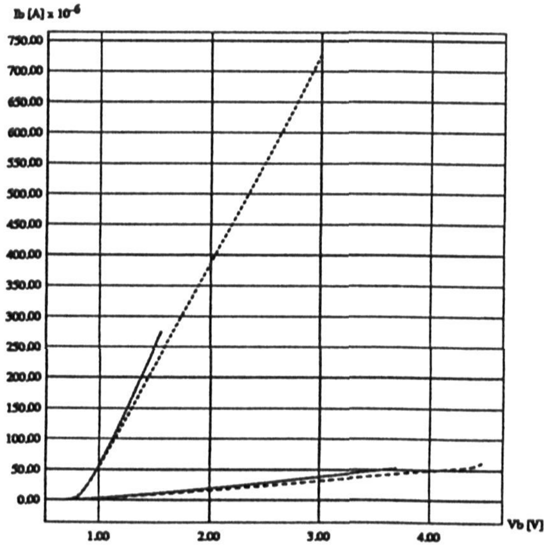

Fig. 15: Base current I_B vs. base-emitter voltage V_{BE} (with $V_{CE} = -5\,V$).

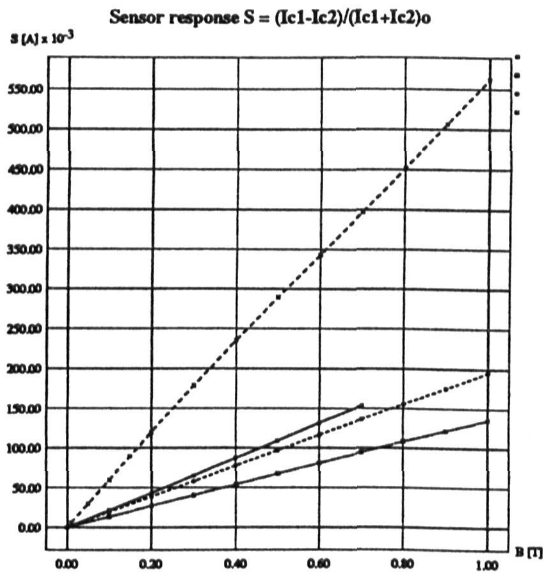

Fig. 16: Sensor response vs. magnetic field.

In both of the above figures, the line types denote:

——— : $d_{EC} = 16\,\mu m$, confined buried layer

·········· : $d_{EC} = 16\,\mu m$, extended buried layer

- - - - : $d_{EC} = 32\,\mu m$, confined buried layer

-----· : $d_{EC} = 32\,\mu m$, extended buried layer

where d_{EC} is the emitter-collector distance.

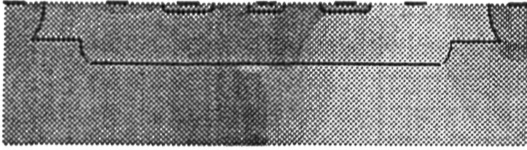

Fig. 17: Change of electric potential at $B = 1.0\,T$ (extended buried layer).

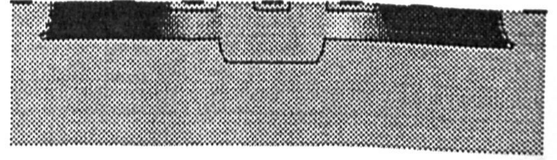

Fig. 18: Change of electric potential at $B = 1.0\,T$ (confined buried layer).

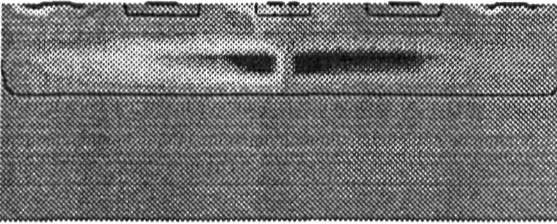

Fig. 19: Change of electron current density at $B = 1.0\,T$ (extended buried layer).

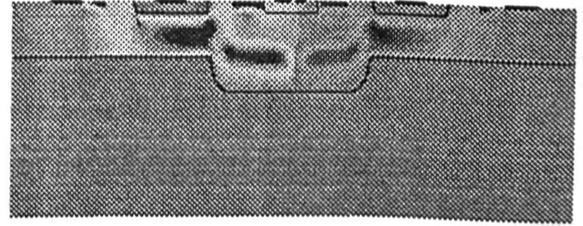

Fig. 20: Change of electron current density at $B = 1.0\,T$ (confined buried layer).

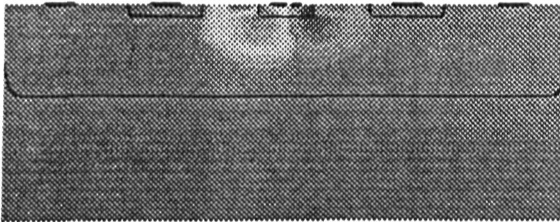

Fig. 21: Change of electron concentration at $B = 1.0\,T$ (extended buried layer).

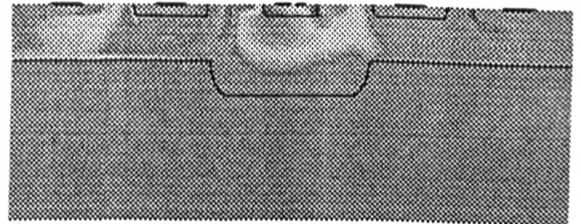

Fig. 22: Change of electron concentration at $B = 1.0\,T$ (confined buried layer).

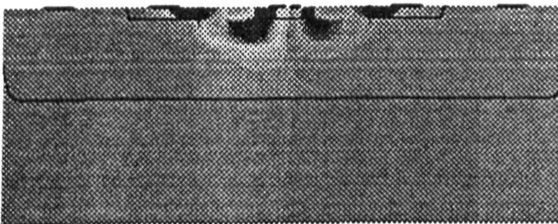

Fig. 23: Change of hole current density at $B = 1.0\,T$ (extended buried layer).

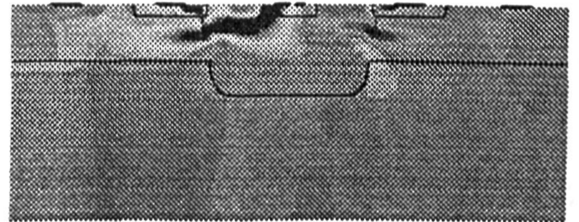

Fig. 24: Change of hole current density at $B = 1.0\,T$ (confined buried layer).

because thereby more room is provided for the drift regions. From Fig. 16 we conclude that sensitivity values of more than 100 %/T are feasible with an optimized design. However, with respect to the signal-to-noise ratio, one should realize that the ratio I_C/I_{sub} deteriorates when choosing a large emitter-collector distance or a laterally confined buried layer, and so we face the problem of a trade-off between high sensitivity and low noise level.

	emitter-collector spacing $16\mu m$	emitter-collector spacing $32\mu m$
confined buried layer	$I_{sub} = 320\mu A$ $I_C = 917\mu A$	$I_{sub} = 811\mu A$ $I_C = 497\mu A$
extended buried layer	$I_{sub} = 81\mu A$ $I_C = 989\mu A$	$I_{sub} = 80\mu A$ $I_C = 499\mu A$

Table 1: Substrate and collector currents of different lateral magnetotransistors, with $I_B = 5\,mA$.

Acknowledgments

The authors gratefully acknowledge the assistance of Dr. N. Bui and his research group at Ascom Microelectronics, Bevaix, Switzerland. They would also like to thank their colleague R. Castagnetti for providing the experimental data necessary for adapting the physical parameter models. The grid generation and the graphical post-processing of the simulation results have been considerably facilitated by the support of S. Müller and M. Westermann at the Integrated Systems Laboratory of the ETH Zurich.

References

[1] W. Heywang, *Halbleiter-Elektronik*, Vol. 17: Sensorik, 4. Aufl., Springer, Berlin (1991), ch. 4.

[2] V. Zieren, *Integrated Silicon Multicollector Magnetotransistors*, PhD Thesis, Delft University of Technology, Delft, The Netherlands (1983).

[3] R. Castagnetti, H. Baltes, A. Nathan, *Noise Correlation and Operating Conditions of Dual-Collector Magnetotransistors*, Sensors & Actuators A26, 363–367 (1991).

[4] R. Castagnetti *et al.*, *PNP Bipolar Magnetotransistor for Sensor Applications*, Transducers '91, San Francisco, USA, 24–27 June 1991.

[5] S. Rudin, G. Wachutka, H. Baltes, *Thermal Effects in Magnetic Microsensor Modeling*, Sensors & Actuators A27, 731–735 (1991).

[6] A. Nathan, H. Baltes, W. Allegretto, *Review of Physical Models for Numerical Simulation of Semiconductor Microsensors*, IEEE Trans. on CAD, CAD-9, 1198–1208 (1990).

[7] J. F. Bürgler, *Discretization and Grid Adaptation in Semiconductor Device Modeling*, PhD Thesis, ETH Zürich, 1990, publ. by Hartung-Gorre, Konstanz, Germany.

[8] R. E. Bank, D. J. Rose, and W. Fichtner, *Numerical Methods for Semiconductor Device Simulation*, IEEE Trans. on Electron Devices, ED-30, 1031–1041 (1983).

[9] W. Allegretto, A. Nathan, H. Baltes, *Numerical Analysis of Magnetic-Field-Sensitive Bipolar Devices*, IEEE Trans. on CAD, CAD-10, 501–511 (1991)

[10] A. Nathan *et al.*, *Noise Correlation in Dual-Collector Magnetotransistors*, IEEE Trans. on Electron Devices, ED-36, 1073–1075 (1991)